

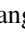


## First-principles study of ferroelectricity, antiferroelectricity, and ferroelasticity in two-dimensional $\gamma$ -AlOOH

Chao Liu <sup>1,2</sup>, Ruiling Gao <sup>1</sup>, Xuli Cheng,<sup>1</sup> Xiaoqing Yang,<sup>1</sup> Guanhua Qin,<sup>1,3</sup> Heng Gao,<sup>1,4</sup> Silvia Picozzi,<sup>2</sup> and Wei Ren <sup>1,3,\*</sup>

<sup>1</sup>Physics Department, State Key Laboratory of Advanced Special Steel, Shanghai Key Laboratory of High Temperature Superconductors, International Centre of Quantum and Molecular Structures, Shanghai University, Shanghai 200444, China

<sup>2</sup>Consiglio Nazionale delle Ricerche (CNR-SPIN), Unità di Ricerca presso Terzo di Chieti, c/o Università G. D'Annunzio, I-66100 Chieti, Italy  
<sup>3</sup>Zhejiang Laboratory, Hangzhou 311100, China

<sup>4</sup>Key Laboratory of Green Fabrication and Surface Technology of Advanced Metal Materials (Anhui University of Technology), Ministry of Education, Maanshan 243002, China;

State Key Laboratory of Surface Physics and Department of Physics, Fudan University, Shanghai 200433, China; and State Key Laboratory of Infrared Physics, Shanghai Institute of Technical Physics, Chinese Academy of Sciences, Shanghai 200083, China



(Received 22 July 2022; accepted 13 February 2023; published 7 March 2023)

The exploration of two-dimensional (2D) ferroic materials and the investigation of ferroic couplings are highly desired in view of the design of next-generation functional devices. Herein, we report through first-principles calculations that the single-layer  $\gamma$ -AlOOH exhibits intrinsic ferroelectric (FE), antiferroelectric (AFE), and ferroelastic properties. The polarization and antipolarization originate from the orientational displacements of hydrogen atoms actuated by two soft phonon modes of the centrosymmetric phase. We studied a possible FE switching process and the FE-AFE transformation in the cases of monolayer and bulk, resulting in the prediction of a stable bulk AFE phase with similar energy to the FE ground state. Moreover, the  $\gamma$ -AlOOH monolayer shows a giant ferroelastic phase transition capable of efficiently tuning the ferroelectricity, which is able to accomplish a 90° switching of polarization and leads to an FE/AFE quadruple state. Our work adds a unique candidate to the family of 2D ferroics, broadening the platform for the design of ferroic-based devices.

DOI: [10.1103/PhysRevB.107.L121402](https://doi.org/10.1103/PhysRevB.107.L121402)

### I. INTRODUCTION

Ferroelectric (FE) systems with spontaneous polarization that can be switched by external electric field have been a significant field of study for many years, due to their various potential applications for functional electronics [1–4]. Conventional (three-dimensional) ferroelectrics are oxide perovskites, such as BaTiO<sub>3</sub> and PbTiO<sub>3</sub> [5,6], which have been widely investigated both experimentally and theoretically [7–10]. Recently, two-dimensional (2D) FE films have also attracted significant interest, stimulated by the increasing demand for miniaturization [11]. The use of traditional ferroelectrics at the nanoscale is generally hindered by the reduction of polarization in thin films and by the presence of depolarization fields [12]. In this respect, 2D ferroelectrics offer added value, due to their ability to maintain switchable electric polarization even in the presence of size and surface effects, along with reduced depolarization fields. Additionally, we note that size-dependent phenomena may emerge and become dominant in the process of approaching the 2D limit and could change the atomic arrangement and electronic structure of the system, thereby causing ferroelectric features that are significantly different from those of their bulk counterparts. A number of 2D ferroelectric monolayers have been proposed,

for example, group IV chalcogenide SnTe with in-plane polarization [13], binary metal phosphorus trichalcogenides CuInP<sub>2</sub>S<sub>6</sub> with vertical ferroelectricity [14,15], distorted transition metal dichalcogenides 1T-MoS<sub>2</sub> and 1T-MoTe<sub>2</sub> [16,17], In<sub>2</sub>Se<sub>3</sub> with intercorrelated in-plane and out of plane polarization [18,19], as well as MXene structure Sc<sub>2</sub>CO<sub>2</sub> with vertical ferroelectricity and antiferroelectricity [20,21]. Accordingly, the investigation of the ferroelectricity of 2D crystals has become one of the frontiers of condensed matter physics and material science.

As is well known, ferroelectricity requires the switching of electric polarization generated by ionic displacements. According to the arrangement of local polarization directions, ferroic systems with active electric dipolar degrees of freedom can be divided into (i) ferroelectric (i.e., with parallel polarization directions across all the unit cells), (ii) antiferroelectric (AFE) (i.e., with antiparallel polarization directions in the neighboring unit cells, leading to a zero macroscopic polarization) [22], and (iii) ferrielectric (i.e., with antiparallel polarization directions but residual net polarization) [23,24]. Each of the three classes shows unique behavior; for example, the prototype antiferroelectric PbZrO<sub>3</sub> exhibits a stepped hysteresis loop upon change of the electric field, which is valuable for high-density energy storage [25]. At present, 2D antiferroelectric materials have received important attention; for example, the double-layer In<sub>2</sub>Se<sub>3</sub> [26,27] and CuCrP<sub>2</sub>S<sub>6</sub> manifest an antiferroelectric phase [28], and multiple potential

\*renwei@shu.edu.cn

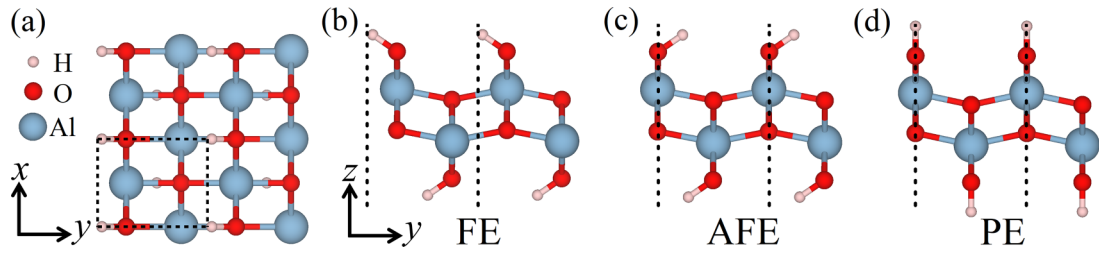


FIG. 1. (a) Top view of monolayer  $\gamma$ -AlOOH in the FE phase. Side views of (b) FE phase, (c) AFE phase, (d) and centrosymmetric PE phase. Aluminum, oxygen, and hydrogen atoms are depicted by the cyan, red, and light pink spheres, respectively. The dashed lines represent the unit cell.

wells arise during the polarization switching, which allows for the realization of antiferroelectric tunnel junctions [29]. Moreover, multiferroicity related to ferroelectricity is also worthy of attention, such as in FE systems also showing ferroelasticity, which further increases their functionalities [30–32]. As a result, novel 2D materials with multiple ferroic characters offer large application potential in nanoelectronics devices.

In this work, we systematically studied the structural and electronic properties of boehmite ( $\gamma$ -AlOOH). Monolayer  $\gamma$ -AlOOH exhibits ferroelectricity, antiferroelectricity, and giant ferroelasticity; its polarization originates from parallel and antiparallel displacements of H atoms. Through studying the FE-AFE transformation in the monolayer, we further proposed a bulk AFE phase that shows a total energy comparable to the FE bulk ground state, and investigated two different transition paths. Electronic structures show that both monolayers in the FE and AFE phases are direct wide band gap semiconductors. Additionally, ferroelasticity manifests a significant tuning effect on ferroelectricity, causing an interesting  $90^\circ$  switching of polarization, leading to a quadruple state characterized by ferroelectricity and antiferroelectricity. The collection of these properties predicted for  $\gamma$ -AlOOH paves the way to applications in ferroelectric field-effect transistors.

## II. METHODS

We performed density functional theory (DFT) simulations, using the Vienna *ab initio* Simulation Package (VASP) [33,34]. The generalized gradient approximation (GGA) based on the Perdew-Burke-Ernzerhof (PBE) functional [35] was employed to treat the exchange-correlation interaction. The projector-augmented-wave (PAW) potentials [36,37] were used to describe the electron-ion interaction. The energy cutoff was selected to be 550 eV for the plane-wave basis set. The Brillouin zones were set to a  $10 \times 10 \times 1$   $k$ -grid mesh and sampled in the  $\Gamma$ -centered scheme. We set the vacuum distance to be larger than 20 Å, in order to avoid spurious periodic interactions. The force convergence standard on each atom was chosen as 0.005 eV/Å and the electronic self-consistent calculations were stopped when the energy difference was smaller than  $10^{-7}$  eV. The van der Waals correction with the D2 method was taken into account in the geometric optimization and exfoliation energy calculations [38]. The phonon spectra were computed based on a density functional theory (DFT) perturbation method with the PHONOPY package [39]. We built a supercell of  $3 \times 3 \times 1$  to

perform phonon calculations, and the force criterion for the ionic step was set to  $10^{-7}$  eV/Å on each atom.

## III. RESULTS AND DISCUSSION

The  $\gamma$ -AlOOH and a range of related materials have been synthesized experimentally to study their crystal structures, phase transitions, and surface properties [40–44]. For bulk  $\gamma$ -AlOOH, the space group is noncentrosymmetric  $Cmc21$  (No. 36), the calculated lattice constants being  $a = 2.88$  Å,  $b = 3.71$  Å, and  $c = 11.86$  Å. Each unit cell contains four aluminum (Al) atoms, eight oxygens (O), and four hydrogens (H). Each Al atom is sixfold-coordinated with surrounding O atoms in an octahedral cage. The  $\gamma$ -AlOOH exhibits a layered configuration with two layers in one unit cell; each upper and lower O atom is connected to an H atom. However, the positions of these H atoms are not directly above/below the O atom; the overall displacement occurs along the in-plane long  $y$  axis, thus leading to intrinsic electric polarization. Therefore,  $\gamma$ -AlOOH is a possible candidate to be included in the class of 2D FE materials.

The optimized crystal structure of the  $\gamma$ -AlOOH monolayer is shown in Fig. 1(a). The calculated lattice constants are  $a = 2.90$  Å,  $b = 3.64$  Å for the case of the monolayer. Notably, the optimized structure still shows a displacement of H atoms similar to that of bulk. Since the inner Al and O atoms constitute a centrosymmetric pattern, the polarization can be reversed by switching the displacements of upper and lower H atoms. When calculating the phonon spectra of the ferroelectric  $\gamma$ -AlOOH monolayer, we find that there is no imaginary frequency vibration mode, which proves the stability of the  $\gamma$ -AlOOH monolayer [45]. Furthermore, we found that the upper and lower hydrogen atoms are highly independent of each other in the case of the monolayer. Therefore, it is feasible that the two types of H atoms displace so as to change the polarization configuration from parallel to antiparallel, thereby leading to an AFE phase. Figure 1(b) displays the side view of the FE phase with parallel displacement directions, and Fig. 1(c) shows a schematic diagram of the AFE phase with antiparallel displacement directions for the upper and lower H atoms, which makes the monolayer exhibit a centrosymmetric structure (space group is  $P2_1/m$ , No. 11) without macroscopic polarity. As is well known, analyzing the vibration modes through the phonon dispersion is an important method to study possible phases of materials. We therefore constructed a centrosymmetric paraelectric (PE) phase in Fig. 1(d) with H atoms located directly above/below

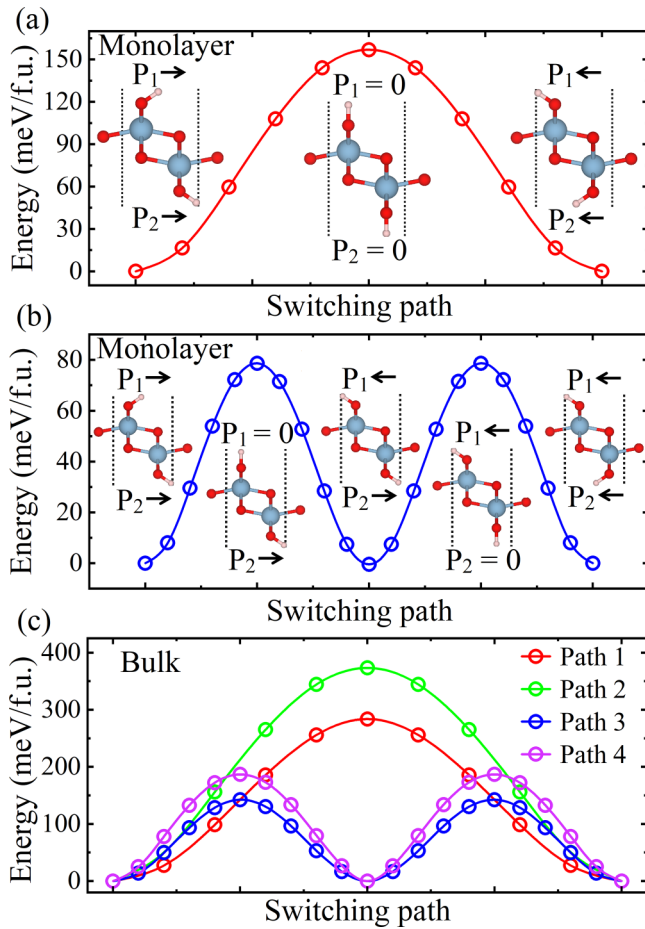


FIG. 2. The energy evolution of two polarization switching paths of FE  $\gamma$ -AlOOH monolayer in two cases: (a) the transition proceeds through an intermediate PE phase; (b) the intermediate phase during the switching path is the AFE configuration. The side views display the structures of initial and final states, and the energy turning point. (c) The energy evolution of four switching paths of  $\gamma$ -AlOOH bulk. Paths 1–4 correspond to different intermediate states. The bulk structure of the energy turning point is shown in the SM [45].

the connected oxygen atoms, and then calculated the phonon spectrum of this phase to analyze the possible vibration modes. As shown in Fig. S1 in the Supplemental Material (SM) [45], there are two proximate imaginary frequencies existing in the phonon spectrum of the PE phase: these vibration modes are related to parallel and antiparallel displacements of upper and lower hydrogen atoms along the long  $y$  axis, which correspond exactly to the FE phase and AFE phase. We also calculated the phonon spectrum to confirm the stability of the AFE phase [45].

In order to study the polarization switching and the relevant energy barrier of the  $\gamma$ -AlOOH monolayer, we constructed two possible switching paths and calculated the energy evolution, as shown in Fig. 2. One intermediate state is the PE phase in Fig. 1(d); the intermediate state of the other path is the AFE phase shown in Fig. 1(c). Only H atoms displace along the  $y$  axis in the process of switching. It is worth noting that H atoms displace in an arc obtained by fixing the length of the O-H bond, which efficiently reduces the energy barrier with

respect to a linear displacement along the  $y$  axis. In Figs. 2(a) and 2(b), the labels  $P_1$  and  $P_2$  represent the local polarization of the upper and lower layers ( $P_{\text{total}} = P_1 + P_2$ ), respectively, and the arrows represent the direction of polarization. We found that the barrier with the intermediate PE phase is about 156.9 meV per formula unit (f.u.). For the other path, the calculated energy barrier is about 78.7 meV/f.u., and the energy evolution shows the shape of a triple potential well, as a result of a stable intermediate AFE phase. This phenomenon has also been reported in 2D AFE materials [27,46,47]. Therefore, we concluded that the FE-AFE transformation is achievable during the ferroelectric switching of the  $\gamma$ -AlOOH monolayer, indicating a higher tunability.

Furthermore, using the modern theory of polarization, i.e., the Berry phase method [48,49], we evaluated the surface polarization  $P_y$  value of  $0.85 \times 10^{-10}$  C/m for the FE phase with respect to the nonpolar configurations. In order to compare with the polarization in bulk, we further employ the volume occupied by one layer of AlOOH in FE bulk to estimate the polarization, and the value is  $P_y = 14.2 \mu\text{C}/\text{cm}^2$ . The nonmetallicity of every configuration on the transition path has been confirmed to ensure the possibility of polarization reversal. Strikingly, in the FE-AFE transformation, we found that the energy of the AFE phase is slightly lower (by 0.45 meV/f.u.) than that of the FE phase, which suggests that the fully relaxed AFE phase with antiparallel displacement of H atoms might be the ground state in the case of the monolayer. This finding prompts us to study the possible AFE phase and FE-AFE transition in  $\gamma$ -AlOOH bulk. These switching barriers are similar to those of some 2D ferroelectric transition metal halides and halogenated oxides [50–52].

According to the analysis of the phonon vibration mode, we studied the displacement of upper H atoms or lower H atoms along the same direction, and constructed the ferroelectric phase, antiferroelectric phase, and paraelectric phase. However, considering a supercell along the  $y$  direction of polarization, the adjacent H atoms on the upper or lower layer can move independently. Combined with the position of H atoms in the ferroelectric and paraelectric phases, four phases (phases 1–4) are obtained, as shown in Fig. S2 [45]. Specifically, the upper and lower layers of phase 1 are antiferroelectric; that is, the displacement direction of adjacent H atoms at the same layer is opposite. Phase 2 is a combination of ferroelectric and paraelectric phases, and the total polarization value is half that of the ferroelectric phase. Phases 3 and 4 are two cases with the combination of antiferroelectric and paraelectric phases. Taking the monolayer ferroelectric phase as a reference, we calculated the relative energy of the four phases. The relative energies of phases 1–4 are 148.90, 92.80, 94.19, and 91.88 eV/f.u., respectively. These four phases can be used as intermediate states of ferroelectric transition, and their potential barriers are lower than that of direct ferroelectric inversion (156.9 meV/f.u.). However, the energy barrier of FE-AFE transition [78.7 meV/f.u. shown in Fig. 2(b)] is lower than that of these phases; this result demonstrates that the transformation path we designed is highly energetically favorable. The investigation of these phases facilitates the proposal of more low-energy states, emphasizes the role of the compensatory displacement modification of the H atoms in the presence of perturbations, and

promotes the exploration of more possible FE-AFE transition paths.

By controlling the displacement of H atoms, we constructed an AFE  $\gamma$ -AIOOH bulk with the same stacking mode as the prototype (Fig. S3 in the SM [45]) and calculated the energy of the bulk FE and AFE phases under complete optimization. The results show that the fully relaxed FE and AFE phases of  $\gamma$ -AIOOH bulk possess almost the same lattice constant and relative energy. In addition, we also studied the possible FE reversal and FE-AFE transition in the bulk. We found two ways to shift the polarization of H atoms, and both FE-PE and FE-AFE transformations could be achieved by these two displacement ways; thus, there is a total of four paths denoted as paths 1–4, respectively. One possibility is that the H atoms make an arc displacement with the connected oxygen atoms as the center of the circle (occurring in paths 1 and 3), which is same as that in the monolayer; the other possibility is to achieve switching through the exchange of interlayered H atoms (occurring in paths 2 and 4). The corresponding energy evolutions are displayed in the Fig. 2(c), and show that the barriers of paths 1–4 are about 283.65, 373.28, 142.35, and 186.65 meV/f.u., respectively. Therefore, the displacement process of paths 1 and 3 is energetically favorable. The structural evolution corresponding to four paths is shown in Fig. S4 [45]. Furthermore, the FE-AFE transitions of paths 3 and 4 indicate that this transition is efficient in minimizing the energy barriers, and the FE-AFE transition is achievable in bulk. We also calculated the lattice constants of the bulk FE and AFE phases, along with the energy difference between two phases, as shown in Table S1 [45]. The energies of the two phases are almost identical, suggesting that the bulk AFE phase is an undiscovered stable structure. On the other hand, the mechanism for bulk polarization switching due to the exchange of interlayered H atoms is similar to that of ferroelectric croconic acid molecular crystal. The  $\gamma$ -AIOOH bulk exhibits a polarization of approximately  $21.7 \mu\text{C}/\text{cm}^2$ , which is comparable to  $\sim 20 \mu\text{C}/\text{cm}^2$  of croconic acid [53], and larger than that of the FE monolayer ( $14.2 \mu\text{C}/\text{cm}^2$ ). We also note that the calculated cleavage energy is  $1.15 \text{ J}/\text{m}^2$  (see Fig. S5 [45]), which is higher than that of van der Waals layered materials ( $0.39 \text{ J}/\text{m}^2$  of graphite [54]). Consequently,  $\gamma$ -AIOOH exhibits a stronger interlayer interaction that plays an important role in the interlayered exchange of H atoms. The prediction of the bulk AFE phase calls for possible experimental confirmation.

The band structures of the FE and AFE phases of the monolayer and bulk  $\gamma$ -AIOOH are calculated. We presented the band structures and partial density of states (PDOS) of the FE phases of bulk and monolayer in Fig. 3, and the band structures of the AFE phases are displayed in Fig. S6 in the SM [45]. As mentioned before, the FE and AFE phases show considerably close energies, and H is the sole element that exhibits different displacement direction in terms of crystal structure. Consequently, the electronic structures of the two phases show a lot in common. For example, both monolayer structures exhibit direct wide band gaps at the  $\Gamma$  point. The band gap of the FE monolayer is about 4.19 eV, and the AFE monolayer shows a close gap value (4.21 eV). For the FE and predicted AFE phases of  $\gamma$ -AIOOH bulk, the band results indicate a direct band gap of 5.24 eV, which is more than 1 eV

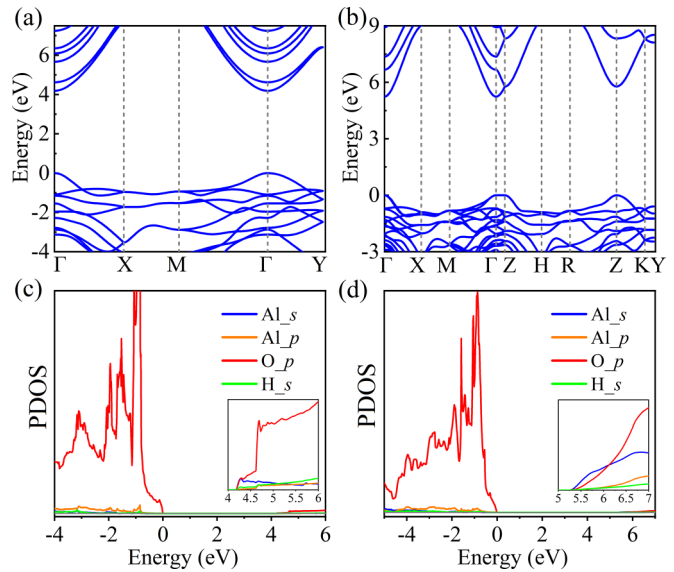


FIG. 3. Panels (a,b) display the band structures of monolayer and bulk FE phases, respectively. Panels (c,d) show the corresponding partial density of states, respectively. The insets in (c,d) are zoomed-in diagrams of the conduction band part. The Fermi level is set to zero.

larger than that of the monolayer. This difference suggests the effect of considerable interlayer interaction on electronic structure, corresponding to high cleavage energy. The band structure differences suggest that constructing heterojunctions and multilayer structures is a feasible approach for band engineering.

In terms of PDOS, the *s* and *p* orbitals of Al atoms, the *p* orbitals of O atoms, and the *s* orbitals of H atoms are considered when analyzing the contribution of atomic orbitals to band dispersion. For both bulk and monolayer FE phases, the O *p* orbitals play a significant effect in the valence band. The contribution of the Al *s* orbital is lower than Al *p* orbitals in the valence band, while the opposite is true in the conduction band. The contribution of H atoms is negligible in the energy range shown. Notably, in the enlarged view of Fig. 3(d), the contribution of the Al *s* orbital of the bulk FE phase is larger than that of the O *p* orbital at the conduction band minimum. Moreover, with only the displacement direction of the H atoms changing, the FE and AFE phases exhibit quite different distributions in terms of *p* orbitals of O atoms in the valence band. Analysis of the electronic structure helps to understand the similarities and differences of the FE and AFE phases in bulk and monolayer, and expand the connection between the FE-AFE switching and the electronic properties.

Interestingly, we discovered that  $\gamma$ -AIOOH exhibits a striking ferroelastic phase transition, and this transition produces an important tuning of the electric polarization, resulting in unique ferroic states. Ferroelasticity is defined by the existence of several equally stable orientation variants that allow the change from one variant to another; in this respect, relevant works on polarized modulation have been reported in 2D few layers and three-dimensional bulk [47,55–59]. Due

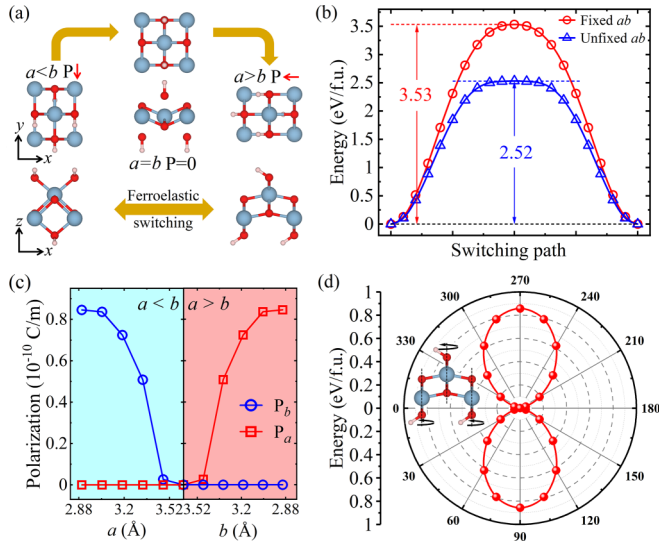


FIG. 4. (a) Schematic diagram of the ferroelastic transition of  $\gamma$ -AIOOH, along with the transformation of polarization directions before and after the ferroelastic transition. (b) The switching barriers for the ferroelastic phase transition. (c) Variation of polarization along the  $x$  and  $y$  axes as a function of the lattice constant  $a$ . (d) The energy evolution during the H atoms' in-plane rotation around the vertical axis perpendicular to the  $xy$  plane (in the case of  $a < b$ ). The energy minimum is set to 0 as a reference (H atoms are along the  $y$  axis). The inset is a schematic diagram of the displacement paths of the H atoms.

to the specific orthorhombic structure of  $\gamma$ -AIOOH, there are two equivalent ground states with the same configuration and energy, and these two equivalent ground states display opposite lattice constants of  $a$  and  $b$ . Figure 4(a) shows the initial, final, and intermediate states of ferroelastic transition of the monolayer. We took the phase with the short  $x$  axis as the initial state, through applying uniaxial strain (tensile strain on the short axis or compressive strain on the long axis), keeping the perimeter of the unit cell unchanged, with the original short lattice transformed into the long lattice, and realizing the ferroelastic transformation. The transition process goes through the paraelastic phase shown in Fig. 4(a), whose tetragonal lattice constants are  $a = b = 3.27 \text{ \AA}$ , i.e., equal to the average value of the initial  $a$  and  $b$ . Figure 4(b) elucidates the barrier for the ferroelastic phase transition. Here we used two intermediate phases with different lattice constants, one of which is the mentioned phase with fixed perimeter. The corresponding barrier for the transition path is  $3.53 \text{ eV/f.u.}$  The other path is obtained by scanning different lattice constants to obtain the intermediate phase with the lowest energy (i.e., unfixed perimeter), which effectively reduces the potential barrier for the switching. We identified  $3.62 \text{ \AA}$  as the optimal lattice constant of the intermediate phase, which requires a maximum tensile strain of 25% on the short axis, while the long axis shrinks by about 0.6%. We further calculated this switching barrier to be  $2.52 \text{ eV/f.u.}$ , which is about  $1 \text{ eV/f.u.}$  lower than the previous one; thus the second path is more favorable according to the principle of minimal energy. Consequently, combined with ferroelectricity,  $\gamma$ -AIOOH indicates

significant multiferroicity, since it is both ferroelastic and ferroelectric at the same time.

In addition, we demonstrated that the interaction of ferroelectricity and ferroelasticity causes interesting phenomena, such as the  $90^\circ$  and  $270^\circ$  rotation of polarization, as shown in Fig. 4(a). We mentioned that the displacement of the H atoms occurs in an overall parallel and antiparallel direction along the long axis, resulting in an FE or AFE reversal ( $180^\circ$ ). Considering the interplay between ferroelastic transition and ferroelectric polarization, the polarization tends to be zero in the ferroelastic intermediate phase. In the case of  $a > b$ , the polarization must align towards the finally longer  $x$  axis to reduce the system; the phase with polarization towards the  $x$  axis also possesses FE bistable states. Therefore, the FE polarization realizes  $90^\circ$  or  $270^\circ$  switching of direction under the operation of the ferroelastic transition, thereby leading to FE quadruple states with polarization in four directions, and homologous quadruple antiferroelectric states. The property of  $90^\circ$  switching polarization also occurs in other 2D materials with ferroelectricity and ferroelasticity [47,51]. Figure 4(c) testifies the polarized magnitude along the  $x$  and  $y$  axes as a function of the  $x$ -axis length ( $a$ ) during the ferroelastic transition. Furthermore, to demonstrate that the polarization has to be oriented towards the long axis to maintain the structural stability, we calculated the energy evolution of the H atoms in the process of in-plane rotation around a defined axis, which is perpendicular to the  $xy$  plane and passes through the nearest neighbor O atoms. The schematic diagram and results are displayed in Fig. 4(d). The lowest energy is when the H atoms are oriented towards the long axis ( $0^\circ$  and  $180^\circ$ ) and is set to zero as a reference. The system energy keeps rising and reaches the highest point with the polarization along the short axis ( $90^\circ$  and  $270^\circ$ ), which is about  $0.86 \text{ eV/f.u.}$  higher than the lowest energy. These results imply that the polarization is always directed towards the long axis for structural stability, consistent with our previous discussion.

#### IV. CONCLUSION

In summary, using first-principles calculations, we investigated the ferroelectricity, antiferroelectricity, and ferroelasticity of the  $\gamma$ -AIOOH monolayer. The origin of polarization lies in the group-oriented displacement of H atoms at the top and bottom of the monolayer, and the FE-AFE transformation is realized through the parallel and antiparallel displacement of H atoms. We clarified that the AFE phase shows a lower energy than the FE phase, and predicted a bulk AFE phase that exhibits comparable energy with the natural FE phase; furthermore, we proposed two FE-AFE transformation ways based on the strong interlayer interaction. The  $\gamma$ -AIOOH monolayer is a direct wide band gap semiconductor with a calculated band gap of  $4.19 \text{ eV}$  for the FE phase and a slightly larger gap of  $4.21 \text{ eV}$  for the AFE phase. In addition, the monolayer shows giant ferroelasticity, requiring a maximum tensile strain of 25% to achieve the ferroelastic switching. We studied the interplay between ferroelasticity and ferroelectricity, which enables a  $90^\circ$  conversion of the polarization through a ferroelastic transition and derive FE and AFE quadruple states. Our results bring an additional member to the 2D FE family, broaden the functional applications of  $\gamma$ -AIOOH,

and provide a route for the discovery and design of new FE materials.

### ACKNOWLEDGMENTS

This work was supported by the National Natural Science Foundation of China (Grants No. 12074241, No. 11929401, and No. 52130204); the Science and Technology Commission of Shanghai Municipality (Grants No. 22XD1400900, No. 20501130600, No. 21JC1402700, and No. 21JC1402600); the High Performance Computing Center, Shanghai University; and the Key Research Project of Zhejiang Laboratory (Grant No. 2021PE0AC02). S.P. acknowledges financial support from the Italian Ministry for Research and Education through

the PRIN-2017 project ‘‘TWEET: Towards Ferroelectricity in Two Dimensions’’ (IT-MIUR Grant No. 2017YCTB59). C.L. acknowledges the support of the China Scholarship Council. H.G. acknowledges the supports from the Shanghai Sailing Program (Grant No. 22YF1413300) of the Shanghai Municipal Science and Technology Commission Program; the open projects of Key Laboratory of Green Fabrication and Surface Technology of Advanced Metal Materials (Anhui University of Technology); the Ministry of Education (Grant No. GFST2022KF08); State Key Laboratory of Surface Physics (Fudan University) (Grant No. KF2022\_10); and State Key Laboratory of Infrared Physics, Shanghai Institute of Technical Physics, Chinese Academy of Sciences (Grant No. SITP-NLIST-YB-2022-08).

- 
- [1] A. V. Bune, V. M. Fridkin, S. Ducharme, L. M. Blinov, S. P. Palto, A. V. Sorokin, S. G. Yudin, and A. Zlatkin, *Nature (London)* **391**, 874 (1998).
- [2] J. Junquera and P. Ghosez, *Nature (London)* **422**, 506 (2003).
- [3] M. Dawber, K. M. Rabe, and J. F. Scott, *Rev. Mod. Phys.* **77**, 1083 (2005).
- [4] D. D. Fong, G. B. Stephenson, S. K. Streiffer, J. A. Eastman, O. Auciello, P. H. Fuoss, and C. Thompson, *Science* **304**, 1650 (2004).
- [5] J. Paul, T. Nishimatsu, Y. Kawazoe, and U. V. Waghmare, *Phys. Rev. Lett.* **99**, 077601 (2007).
- [6] M. Okuyama and Y. Hamakawa, *Ferroelectrics* **63**, 243 (1985).
- [7] Z. G. Gui, S. Prosandeev, and L. Bellaiche, *Phys. Rev. B* **84**, 214112 (2011).
- [8] F. Li, M. J. Cabral, B. Xu, Z. X. Cheng, E. C. Dickey, J. M. LeBeau, J. L. Wang, J. Luo, S. Taylor, W. Hackenberger, L. Bellaiche, Z. Xu, L. Q. Chen, T. R. Shrout, and S. J. Zhang, *Science* **364**, 264 (2019).
- [9] Z. J. Jiang, R. Z. Zhang, D. W. Wang, D. Sichuga, C. L. Jia, and L. Bellaiche, *Phys. Rev. B* **89**, 214113 (2014).
- [10] Y. R. Yang, M. Stengel, W. Ren, X. H. Yan, and L. Bellaiche, *Phys. Rev. B* **86**, 144114 (2012).
- [11] Z. Guan, H. Hu, X. W. Shen, P. H. Xiang, N. Zhong, J. H. Chu, and C. G. Duan, *Adv. Electron. Mater.* **6**, 1900818 (2020).
- [12] C. J. Cui, F. Xue, W. J. Hu, and L. J. Li, *npj 2D Mater. Appl.* **2**, 18 (2018).
- [13] K. Chang, J. W. Liu, H. C. Lin, N. Wang, K. Zhao, A. M. Zhang, F. Jin, Y. Zhong, X. P. Hu, W. H. Duan, Q. M. Zhang, L. Fu, Q. K. Xue, X. Chen, and S. H. Ji, *Science* **353**, 274 (2016).
- [14] A. Belianinov, Q. He, A. Dziaugys, P. Maksymovych, E. Eliseev, A. Borisevich, A. Morozovska, J. Banys, Y. Vysochanskii, and S. V. Kalinin, *Nano Lett.* **15**, 3808 (2015).
- [15] M. W. Si, A. K. Saha, P. Y. Liao, S. J. Gao, S. M. Neumayer, J. Jian, J. K. Qin, N. B. Wisinger, H. Y. Wang, P. Maksymovych, W. Z. Wu, S. K. Gupta, and P. D. Ye, *ACS Nano* **13**, 8760 (2019).
- [16] S. N. Shirodkar and U. V. Waghmare, *Phys. Rev. Lett.* **112**, 157601 (2014).
- [17] S. G. Yuan, X. Luo, H. L. Chan, C. C. Xiao, Y. W. Dai, M. H. Xie, and J. H. Hao, *Nat. Commun.* **10**, 1775 (2019).
- [18] W. J. Ding, J. B. Zhu, Z. Wang, Y. F. Gao, D. Xiao, Y. Gu, Z. Y. Zhang, and W. G. Zhu, *Nat. Commun.* **8**, 14956 (2017).
- [19] C. J. Cui, W. J. Hu, X. G. Yan, C. Addiego, W. P. Gao, Y. Wang, Z. Wang, L. Z. Li, Y. C. Cheng, P. Li, X. X. Zhang, H. N. Alshareef, T. Wu, W. G. Zhu, X. Q. Pan, and L. J. Li, *Nano Lett.* **18**, 1253 (2018).
- [20] A. Chandrasekaran, A. Mishra, and A. K. Singh, *Nano Lett.* **17**, 3290 (2017).
- [21] J. B. Pang, R. G. Mendes, A. Bachmatiuk, L. Zhao, H. Q. Ta, T. Gemming, H. Liu, Z. F. Liu, and M. H. Rummeli, *Chem. Soc. Rev.* **48**, 72 (2019).
- [22] D. J. Singh, *Phys. Rev. B* **52**, 12559 (1995).
- [23] S. Dong, J. M. Liu, and E. Dagotto, *Phys. Rev. Lett.* **113**, 187204 (2014).
- [24] Z. Q. Fu, X. F. Chen, Z. Q. Li, T. F. Hu, L. L. Zhang, P. Lu, S. J. Zhang, G. S. Wang, X. L. Dong, and F. F. Xu, *Nat. Commun.* **11**, 3809 (2020).
- [25] B. K. Mani, S. Lisenkov, and I. Ponomareva, *Phys. Rev. B* **91**, 134112 (2015).
- [26] C. F. Li, W. J. Zhai, Y. Q. Li, Y. S. Tang, J. H. Zhang, P. Z. Chen, G. Z. Zhou, X. M. Cui, L. Lin, Z. B. Yan, X. K. Huang, X. P. Jiang, and J. M. Liu, *New J. Phys.* **23**, 083019 (2021).
- [27] C. Xu, Y. C. Chen, X. B. Cai, A. Meingast, X. Y. Guo, F. K. Wang, Z. Y. Lin, T. W. Lo, C. Maunders, S. Lazar, N. Wang, D. Y. Lei, Y. Chai, T. Y. Zhai, X. Luo, and Y. Zhu, *Phys. Rev. Lett.* **125**, 047601 (2020).
- [28] M. A. Susner, R. Rao, A. T. Pelton, M. V. McLeod, and B. Maruyama, *Phys. Rev. Mater.* **4**, 104003 (2020).
- [29] J. Ding, D. F. Shao, M. Li, L. W. Wen, and E. Y. Tsymlal, *Phys. Rev. Lett.* **126**, 057601 (2021).
- [30] C. Xu, J. F. Mao, X. Y. Guo, S. R. Yan, Y. C. Chen, T. W. Lo, C. S. Chen, D. Y. Lei, X. Luo, J. H. Hao, C. X. Zheng, and Y. Zhu, *Nat. Commun.* **12**, 3665 (2021).
- [31] M. H. Wu and X. C. Zeng, *Nano Lett.* **16**, 3236 (2016).
- [32] T. Zhang, Y. D. Ma, L. Yu, B. B. Huang, and Y. Dai, *Mater. Horiz.* **6**, 1930 (2019).
- [33] G. Kresse and J. Furthmüller, *Phys. Rev. B* **54**, 11169 (1996).
- [34] G. Kresse and J. Furthmüller, *Comput. Mater. Sci.* **6**, 15 (1996).
- [35] J. P. Perdew, K. Burke, and M. Ernzerhof, *Phys. Rev. Lett.* **77**, 3865 (1996).
- [36] P. E. Blöchl, *Phys. Rev. B* **50**, 17953 (1994).
- [37] G. Kresse and D. Joubert, *Phys. Rev. B* **59**, 1758 (1999).
- [38] S. Grimme, *J. Comput. Chem.* **27**, 1787 (2006).
- [39] A. Togo and I. Tanaka, *Scr. Mater.* **108**, 1 (2015).

- [40] W. Milligan and J. McAtee, *J. Phys. Chem.* **60**, 273 (1956).
- [41] Y. G. Xia, L. Zhang, X. L. Jiao, and D. R. Chen, *Phys. Chem. Chem. Phys.* **15**, 18290 (2013).
- [42] A. Cedillo, M. Torrent, and P. Cortona, *J. Phys.: Condens. Matter* **28**, 185401 (2016).
- [43] P. Raybaud, M. Digne, R. Iftimie, W. Wellens, P. Euzen, and H. Toulhoat, *J. Catal.* **201**, 236 (2001).
- [44] B. Z. Zhao, X. J. Xie, S. L. Xu, Y. Pan, B. X. Yang, S. H. Guo, T. Wei, H. Q. Su, H. B. Wang, X. Q. Chen, V. P. Dravid, L. Huang, and W. Huang, *Adv. Mater.* **28**, 6665 (2016).
- [45] See Supplemental Material at <http://link.aps.org/supplemental/10.1103/PhysRevB.107.L121402> for the phonon spectra of the PE, FE, and AFE phases; (ii) the side views of four constructed supercells; (iii) the views of AlOOH bulk; (iv) the four FE switching ways of bulk  $\gamma$ -AlOOH; the cleavage energy of the FE phase; (vi) band structures of monolayer and bulk  $\gamma$ -AlOOH AFE phases; (vii) the high-symmetry points in the Brillouin zone; (viii) the calculated lattice constants of bulk  $\gamma$ -AlOOH.
- [46] Z. Guan, Y. F. Zhao, X. T. Wang, N. Zhong, X. Deng, Y. Z. Zheng, J. J. Wang, D. D. Xu, R. R. Ma, F. Y. Yue, Y. Cheng, R. Huang, P. H. Xiang, Z. M. Wei, J. H. Chu, and C. G. Duan, *ACS Nano* **16**, 1308 (2022).
- [47] X. K. Feng, X. K. Ma, L. Sun, J. Liu, and M. W. Zhao, *J. Mater. Chem. C* **8**, 13982 (2020).
- [48] R. D. King-Smith and D. Vanderbilt, *Phys. Rev. B* **47**, 1651 (1993).
- [49] R. Resta, *Ferroelectrics* **136**, 51 (1992).
- [50] M. Xu, C. Huang, Y. Li, S. Liu, X. Zhong, P. Jena, E. Kan, and Y. Wang, *Phys. Rev. Lett.* **124**, 067602 (2020).
- [51] L. F. Lin, Y. Zhang, A. Moreo, E. Dagotto, and S. Dong, *Phys. Rev. Lett.* **123**, 067601 (2019).
- [52] Y. Zhao, L. Lin, Q. Zhou, Y. Li, S. Yuan, Q. Chen, S. Dong, and J. Wang, *Nano Lett.* **18**, 2943 (2018).
- [53] S. Horiuchi, Y. Tokunaga, G. Giovannetti, S. Picozzi, H. Itoh, R. Shimano, R. Kumai, and Y. Tokura, *Nature (London)* **463**, 789 (2010).
- [54] W. Wang, S. Y. Dai, X. D. Li, J. R. Yang, D. J. Srolovitz, and Q. S. Zheng, *Nat. Commun.* **6**, 7853 (2015).
- [55] T. Zhang, Y. Liang, X. L. Xu, B. B. A. Huang, Y. Dai, and Y. D. Ma, *Phys. Rev. B* **103**, 165420 (2021).
- [56] L. He, P. P. Shi, L. Zhou, Z. B. Liu, W. Zhang, and Q. Ye, *Chem. Mater.* **33**, 6233 (2021).
- [57] X. N. Ma, C. Liu, W. Ren, and S. A. Nikolaev, *npj Comput. Mater.* **7**, 177 (2021).
- [58] S. H. Baek, H. W. Jang, C. M. Folkman, Y. L. Li, B. Winchester, J. X. Zhang, Q. He, Y. H. Chu, C. T. Nelson, M. S. Rzechowski, X. Q. Pan, R. Ramesh, L. Q. Chen, and C. B. Eom, *Nat. Mater.* **9**, 309 (2010).
- [59] R. J. Xu, S. Liu, I. Grinberg, J. Karthik, A. R. Damodaran, A. M. Rappe, and L. W. Martin, *Nat. Mater.* **14**, 79 (2015).